Electrostatic mask for active targets

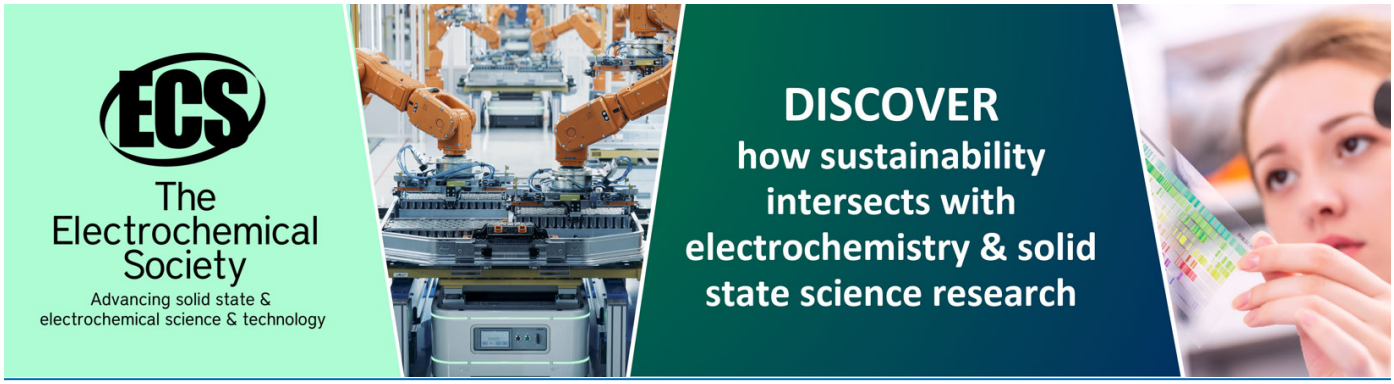

PUBLISHED BY IOP PUBLISHING FOR SISSA

RECEIVED: *October 25, 2011*
ACCEPTED: *December 9, 2011*
PUBLISHED: *January 9, 2012*

Electrostatic mask for active targets

J. Pancin,[a,1] J. Gibelin,[b] M. Goth,[b] P. Gangnant,[a] J.-F. Libin,[a] R. Raabe,[a] T. Roger,[a] and P. Roussel-Chomaz[a]

[a] *GANIL,CEA/DSM-CNRS/IN2P3, Caen, France*
[b] *LPC-ENSICAEN, CNRS/IN2P3 et Université de Caen, Caen, France*

E-mail: pancin@ganil.fr

ABSTRACT: Active gas targets have been used in nuclear physics since 30 years. They are promising systems in view of the new exotic beams soon available at facilities like SPIRAL2 or FAIR, but the system can still be improved. One of the main limitation is the dynamic range in energy deposition. The energy deposited per unit length can be 3 decades higher for the beam than for the light reaction products and the risk to saturate the electronics or that the detector spark are not negligible. A simple solution using a wire plane to mask partially the beam is presented here. Some simulation has been realized and some experimental results are shown confirming the feasibility of this wire tunable mask. The mask can be used from full transparency to full opacity without degrading neither the drift electric field of the chamber nor the performances of detection of the beam or the light products.

KEYWORDS: Time projection Chambers (TPC); Gaseous detectors; Heavy-ion detectors

[1] Corresponding author.

doi:10.1088/1748-0221/7/01/P01006

2012 JINST 7 P01006

Contents

2012 JINST 7 P01006

1 Introduction

Radioactive isotope beams are widely used to study nuclear astrophysics and nuclear structure. However, the intensity of these beams are usually many orders of magnitude lower than stable beams. The reaction rate can be optimized by increasing the thickness of the target but the detection of the low energy reaction products suffers in that case from large energy and angular uncertainties. A good solution is the active gas target where the gas is both used as target and as ionization source for detection. The detection system is hence very efficient, due to its large solid angle and low energy detection threshold. The thickness of the gas target can be easily increased by changing the pressure. The detection in coincidence of the beam and the reaction products improves the reaction vertex reconstruction and allows a good background rejection. While IKAR is the first example of this type of detector [1], very interesting results have been recently obtained with the active target MAYA [2].

The dynamic range in energy, that is to say the range between the smallest and the highest detectable charge is of primary importance to perform accurate trajectory reconstruction. One has to take care to be sensitive enough to detect at the same time the lowest mass particles and the heaviest ones without saturating neither the electronics nor the detector. For instance, for a reaction like d(^{56}Ni,^{56}Ni*)d' at 50 MeV/nucleon [3], the ^{56}Ni beam had to be shielded in order to lower the detection threshold for the deuterium by increasing the detector gain without saturating the electronics. Furthermore it is not only a problem of electronics since the charge density a gaseous detector can deal with is limited. Some solutions allowing to observe at the same time the beam and the secondary light particles have hence to be proposed. The solution described here consists in a wire plane placed just below the beam and playing the role of an electrostatic mask. It is

quite a promising solution due to its simplicity, efficiency and adaptability. In a first section, the active target MAYA and the specific problem of energy dynamics are presented. The mask and a comparison between simulations and experimental results are described in the second section.

2 Active targets

The active targets are gaseous detectors that work as time-projection chambers (TPC), recording the tracks of ionizing particles traversing the gas volume. Exotic particle-emission decay channels can be studied by stopping the radioactive nuclei in the gas [4]; alternatively, by using the nuclei of the gas atoms as target nuclei, it becomes possible to study reactions induced by low intensity beams of exotic ions [5]. The technique yields high efficiencies and allows the use of thick target without loss in resolution. Of particular importance is the low detection threshold. Applications of active targets are wide, ranging from direct reactions, such as inelastic scattering and nucleon transfer, to resonant reactions, and exotic decay modes.

2.1 Scientific interest, examples

The development of new radioactive beams will allow for example studies in the vicinity of ^{80}Zn or ^{132}Sn which is potentially doubly magic nuclei. The studies of single-particle properties and shell structure in this region will constraint shell-model calculations. For example, ^{80}Zn at 8 MeV/nucleon can be used to induce transfer reactions on a deuterium gas filling an active target such as MAYA. Several transfer reactions can be studied like (d,p) at backward angles, or (d,t) at forward angles. The missing-mass method is applied to obtain the level scheme of the heavy partner from the kinematic characteristics of the light recoil. While with a solid target the energy resolution is limited by the target thickness, with an active target high densities of gas target can be used without affecting the vertex and thus the energy resolution. It allows a complete reconstruction of the kinematics since it is possible to detect particles with low energy (notably for backward angles) and it is also very interesting for low intensity exotic beams since it increases the total target thickness.

The dynamic energy range needed to achieve this type of reaction is very large. At a pressure of 1 bar of deuterium gas, the energy loss of the beam is about 700 keV/mm while it can go down to 1 keV/mm for the more energetics protons. Moreover, an energy threshold of 1 keV/mm is generally required since the deposited energy is calculated *a posteriori* from the particle range measurement. Since a factor close to 10^3 is needed in energy dynamics, both the detector and the electronics should be able to cope with it.

The current electronics used on the MAYA detector is based on Gassiplex chips [6], limited to 200 fC per channel and usually recorded on 12 bits. A new system called GET (General Electronic for TPCs) is currently designed (thanks to a french fund ANR-09-BLAN-0203-01). The dynamic charge range can take 4 different values depending on the application and is coded on about 10 effective bits depending on the range (120 fC, 240 fC, 1 pC or 10 pC). For one given range, the ratio between the minimum and the maximum energy deposit that can read the electronics remains around 300 like the Gassiplex chips. This is still not enough to this extreme case of transfer reaction with ^{80}Zn or ^{132}Sn. However, GET will permit to use some channels with different charge range.

2012 JINST 7 P01006

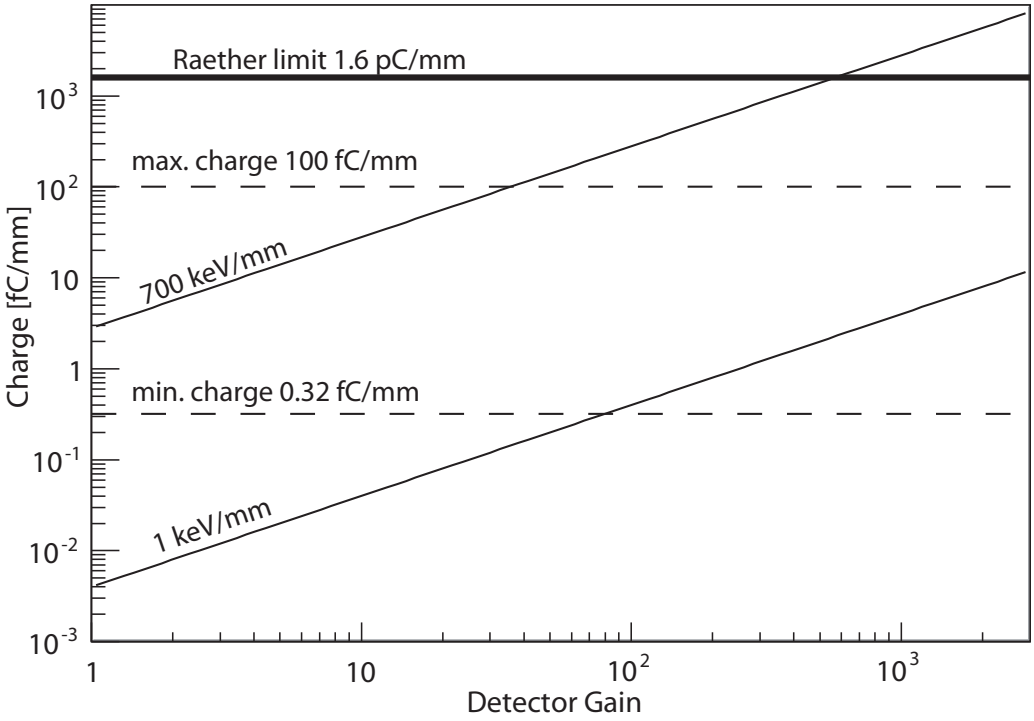

Figure 1. Total charge per mm versus the detector gain for two nuclei, one heavy nucleus with 700 keV/mm and one light nucleus with only 1 keV/mm. The Raether limit and the operating limits of an electronics limited to 200 fC with a dynamic range of 300 are displayed.

Some pads will hence be adapted to detect the heavy nuclei while other pads will be adapted to light nuclei.

Electronics is not the sole limitation: the total charge achievable in an avalanche process is not infinite and is limited to a critical value between 10^6 and 10^7 electrons called the Raether limit [7]. Above this limit, a breakdown can appear and blind the detector or even degrade its performances. This limit takes into account the number of ionization electrons together with the gain. Hence, the maximal achievable gain will be lower with heavy particles than with light particles. The density of the primary ionization electrons is hence an important parameter limiting the maximum gain. Considering that gain measurements are generally performed with X-ray source (like ^{55}Fe with X-rays at 5.9 keV) and that the mean free path of a 6 keV photo-electron is between 0.5 and 1 mm, it seems reasonable to say that in a TPC configuration the maximum charge per millimeter is 10^7/mm (or 1.6 pC/mm).

The figure 1 is an illustration of the different limitations. The total charge per millimeter is plotted versus the detector gain considering two nuclei, an heavy one depositing 700 keV/mm and a light one with only 1 keV/mm (with an energy pair creation W_i of 40 eV). The Raether limit is also displayed showing that the maximum gain achievable before sparking with the heavy nucleus is around 600. The operating limits of an electronics limited to 200 fC with a dynamic range of 300 are shown. Whatever the detector gain is, it seems impossible to detect both the heavy and the light nuclei with an electronic with only one charge range.

2012 JINST 7 P01006

2.2 Description of MAYA

A full description of the detector can be found in [2]. Two main zones compose the detector: an active volume of $28 \times 26 \times 20$ cm^3 where the reaction takes place, and the amplification area where detection and readout occur. The amplification zone consists of a Frisch grid, an anode wire plane below, and a segmented cathode in the lower part. The cathode is segmented 32x32 hexagonal pads of 5 mm side. The pads are arranged in rows both parallel to the anode wires and to the beam. Their signals are individually read and coded *via* Gassiplex electronics and triggered row by row using the above wire signal.

The beam and the reaction products ionize the filling gas along their paths. The electrons released in the ionization process drift toward the amplification area, where they are accelerated around the wires. A mirror charge is induced on the corresponding pads of the segmented cathode and coded individually. Typically the image charge from one avalanche will spread over several pads and the resulting distributions are used to obtain a two dimensional projection of the tracks. Measurements of the drift time of the ionizing electrons down to the amplification wires allow to calculate the vertical position and a complete 3-dimensional reconstruction. For details the reader is referred to ref. [8]. Ancillary detectors, such as Cesium Iodide crystals, silicon, or diamond detectors are usually placed downstream in order to detect particles that do not stop inside the gas volume.

Finally, a collimated one-sided 3α source (mixture of Pu, Am, Cu) has been mounted on a retractable epoxy arm along the transverse axis to the beam. The design of this arm is such that the source can be moved from outside, without opening, and be placed from a position entirely outside the active volume to the center of the detector.

3 An electrostatic mask: solution for dynamics limitations

The gas amplification factor has to be optimized to observe the tracks of the reaction products. Depending on the reaction, they deposit as few as several keV per millimeters, which can be several order of magnitude lower that the energy deposited by the beam. Besides the huge dynamic range it represents for the electronics, there is a non negligible risk of sparking. Considering the mass and the kinetic energy of the beam, it undergoes a low straggling and tends to stay in the center of the detector, even in the case of a nuclear reaction.

The GET electronics will give a partial solution since it will be possible to specify a different charge range for the central pad rows where the beam passes ($1pC$ versus 120 ou 240 fC for the other pads). The detector will be able to cope in that case with both types of energy deposit, as long as the Raether limit is really at 1.6 pC/mm and not below, encroaching the charge range of the central pads. Nevertheless, in the case of MAYA using Gassiplex, an another solution has to be found.

The solution proposed consists in adding in the center of the detector, in the vicinity of the beam trajectory, a device that will partially mask it. One must note that the technique of a total masking was previously used [3], resulting in the beam track not recorded at all. A similar method was also used in gated time projection chambers [9]. However, the purpose was different since the idea was to gate the ions to avoid space charge effect in the drift volume.

The prototype studied here consists in a wire plane along the beam located about 1 cm below, between the beam and the Frisch grid. Its width fits the beam transversal size and is hence limited

2012 JINST 7 P01006

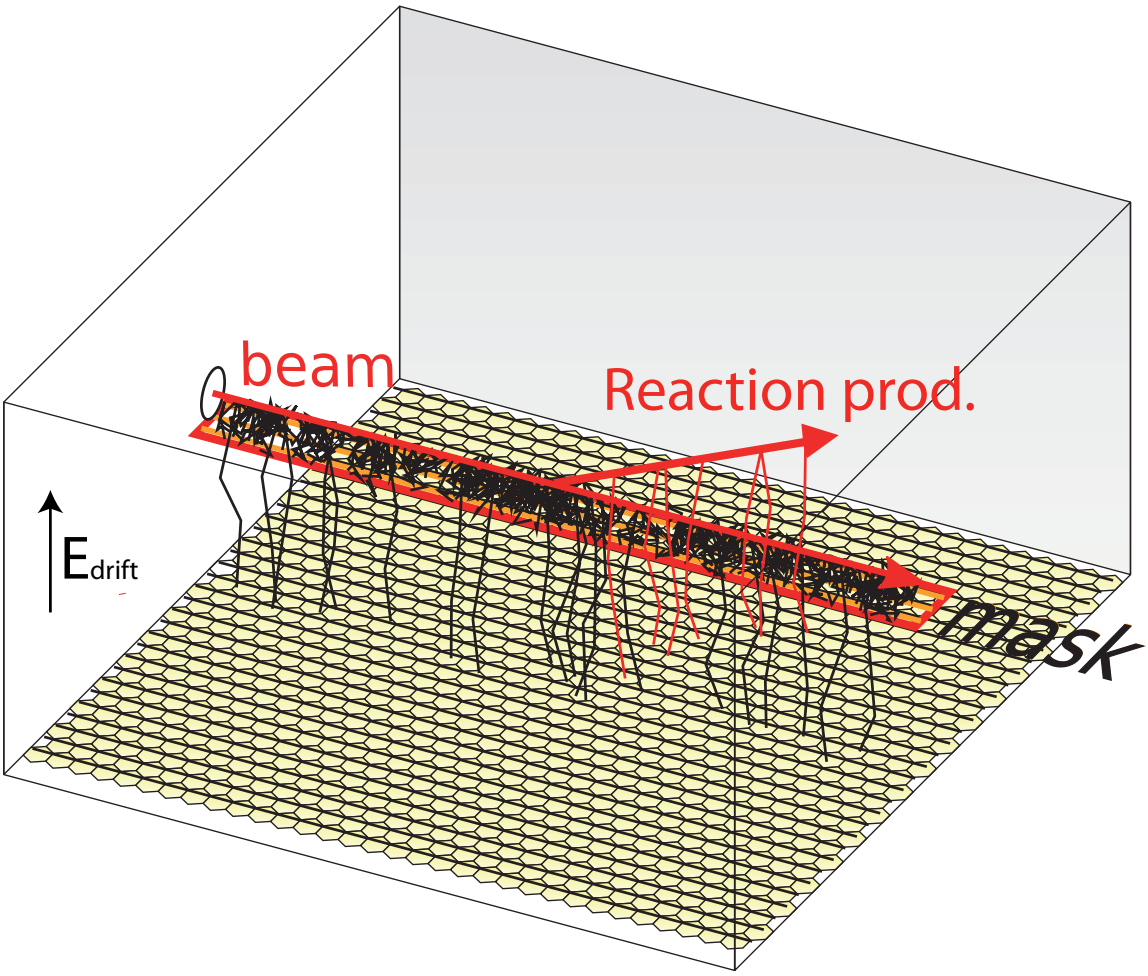

Figure 2. Artist's view of the active target MAYA, restricted to the active gas volume. One can see at the bottom the active honeycomb structure of 32x32 hexagonal pads and the amplification wires. The mask is represented just below the beam trajectory. Random trajectories of the ionization electrons has been generated respectively by the beam and a reaction product.

to the central pads where the beam is detected, so as not to disturb the drift-lines elsewhere. For example, during our tests, we only had 9 wires of 50 μm diameter with a 1 mm pitch. They were pulled along the detector from the entry foils to the diamond beam stopper detector (see figure 2).

In normal conditions, when a complete transparency is required, the wires are polarized at the value imposed by the drift electric field at the height of the mask $V_m = \frac{h_m}{h_d} V_d$ (with h_m the height of the mask, h_d the drift gap size and V_d the drift voltage value). If the beam has to be partially hidden, the same voltage than for full transparency is kept for the edge wires of the mask (so as not to disturb the drift lines) and the bias of the central wires is increased in order to collect the ionization electron from the beam. Figure 3.a shows how the mask is polarized with $-V_m$ the voltage imposed by the field cage and dV the bias to the central wires to decrease the transparency.

2012 JINST 7 P01006

3.1 Simulations

The figure 3.b, 3.c and 3.d present calculations of the drift lines using the GARFIELD software [10]. Electrons are released 1 cm above the wires of the mask and the drift lines are reported on the figures. Figure 3.b is obtained with $-V_m$ everywhere to have a complete transparency. However, to produce this figure, $-V_m$ had to be slightly decreased by 1.5% to obtain straight drift line with no influence from the mask. The field lines are concentric close to the wires and the small voltage decrease permits to repeal these fields lines and keep the drift lines straight. In the two figures 3.c and 3.d, the partial transparency is achieved by decreasing the absolute voltage of the central wires by 2% (varying dV). Diffusion in He+CF_4(1%) is included in figure 3.d to confirm that the behavior of the mask is still correct in more realistic conditions. One sees than the drift lines on the edges of the mask are only slightly perturbed both in full and in partial transparency mode.

The influence of the mask has been calculated by GARFIELD simulations to estimate its transparency and its effect on the electron trajectories when varying the central bias dV. Electrons are uniformly generated in a square of 0.8×0.8 cm^2 centered at 1.5 cm above the mask to simulate the ionization electrons generated by the beam. They are then transported along the electric field, taking diffusion into account. Figure 4 present the results obtained for different dV for 1000 initial electrons. Figures 4.a, b and c are obtained with full transparency ($dV = 0$). The first figure (a) gives the final coordinate (transverse axis to the mask wires or the beam) of the electrons that went through the mask. The transparency is 99.9% and the electrons ends on the amplification wires which are placed every 0.4 cm. The second figure (b) shows the difference between the initial coordinate of the electron and the end (dx). One sees that already in full transparency, a standard variation of 0.15 cm is induced by the pitch of the amplification wires. The results is the same if the mask is removed from the simulation. Figure (c) gives as a reference the initial coordinate of the electrons able to go through the mask.

The figures 4.d and 4.e are obtained with 50% transparency (475 electrons over 1000 have gone through). It is achieved by putting a dV of 1.85% of the nominal value V_m. The shift dx stays below 0.4 cm even if the distribution broadens. The distribution are not uniform anymore since the mask is more efficient in the center due to the $2 \times dV$ of the central mask wires. This effect can be observed on the *xi* histogram (4.e) where the number of electrons in the center has been reduced compared to the number of electrons on the edge (4.c). The effect of the mask is also not uniform due to the pitch of the mask wires and its tendency to focus the electrons which are passing through. However, this is not critical since the beam is never perfectly aligned with the mask and the trajectory is reconstructed with the entire track. The height above the mask at which the electrons are released has no effect. Finally, figures 4.f and 4.g are obtained with only 2% transparency with a dV of 3.7%. Only the electrons on the edges are able to go through and they experienced a shift of 0.4 cm because of this focusing.

The simulations are useful for the design of this mask and indicate that it should work properly. The pitch effect of the mask wires could be reduced by increasing the number of wires but the shape of the potential will always imply that the electrons get focused. However, it has probably no influence on the reconstruction of the track taking into account the shift already imposed by the amplification wires.

2012 JINST 7 P01006

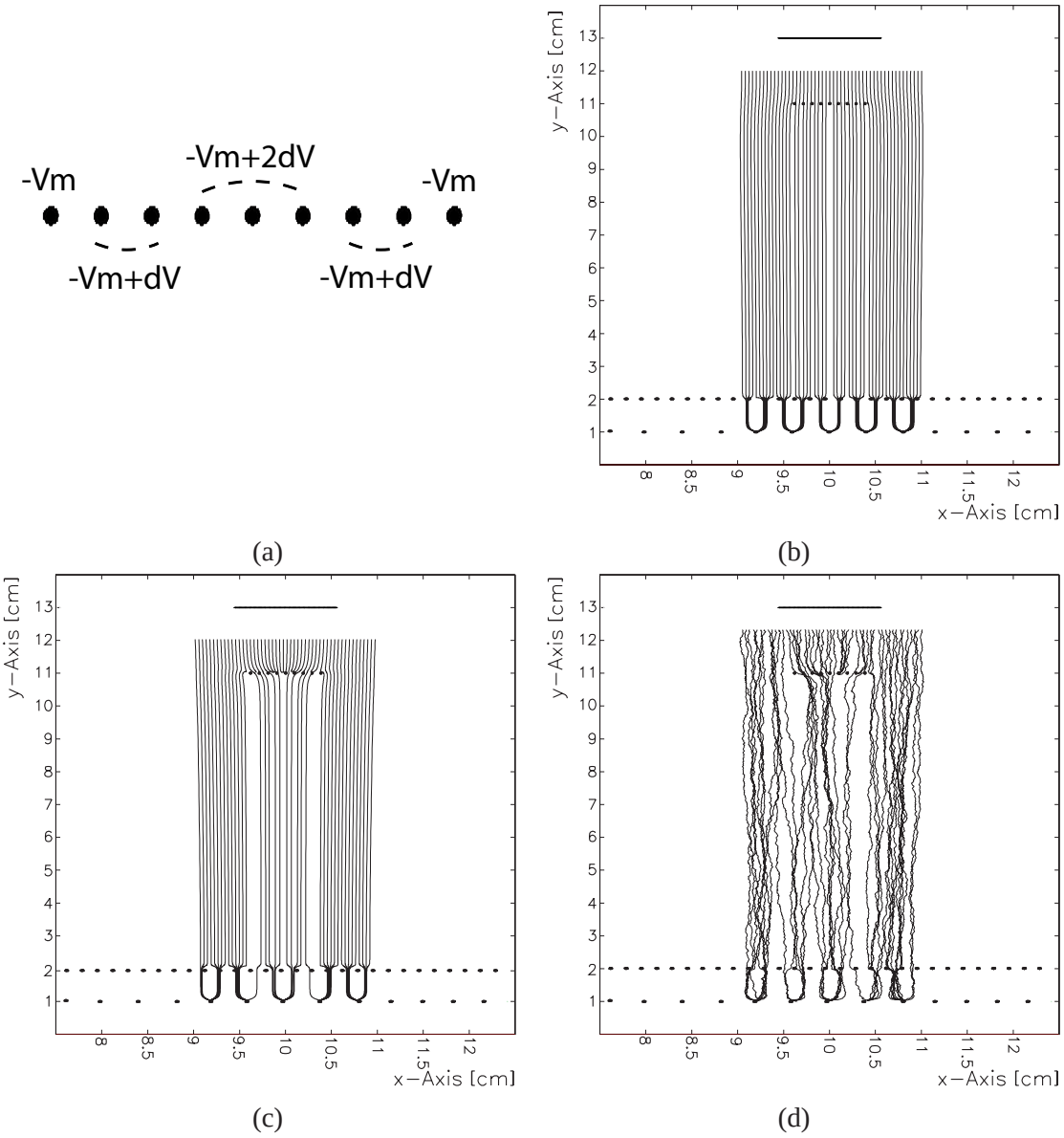

Figure 3. Simulation of electron drift lines in MAYA with the mask: (a) Voltage applied to the mask, (b) total transparency, (c) partial transparency and (d) partial transparency with diffusion in He+CF_4(1%) (The diameter of the wires is not to scale).

3.2 Experimental results and comparison with simulations

Several unwanted effects can arise from the presence of the mask, most of them due to the disturbance of the homogeneous electric field needed in the drift volume. The different tests performed to characterize these effects are presented in the following. These experiments were of two natures:

- some used the α source (of $E_\alpha \approx 5.5$ MeV), thereafter referred as "source runs"
- others ("beam runs") were carried out with a 108 MeV ^{36}Ar beam delivered by the CIME cyclotron in GANIL.

2012 JINST 7 P01006

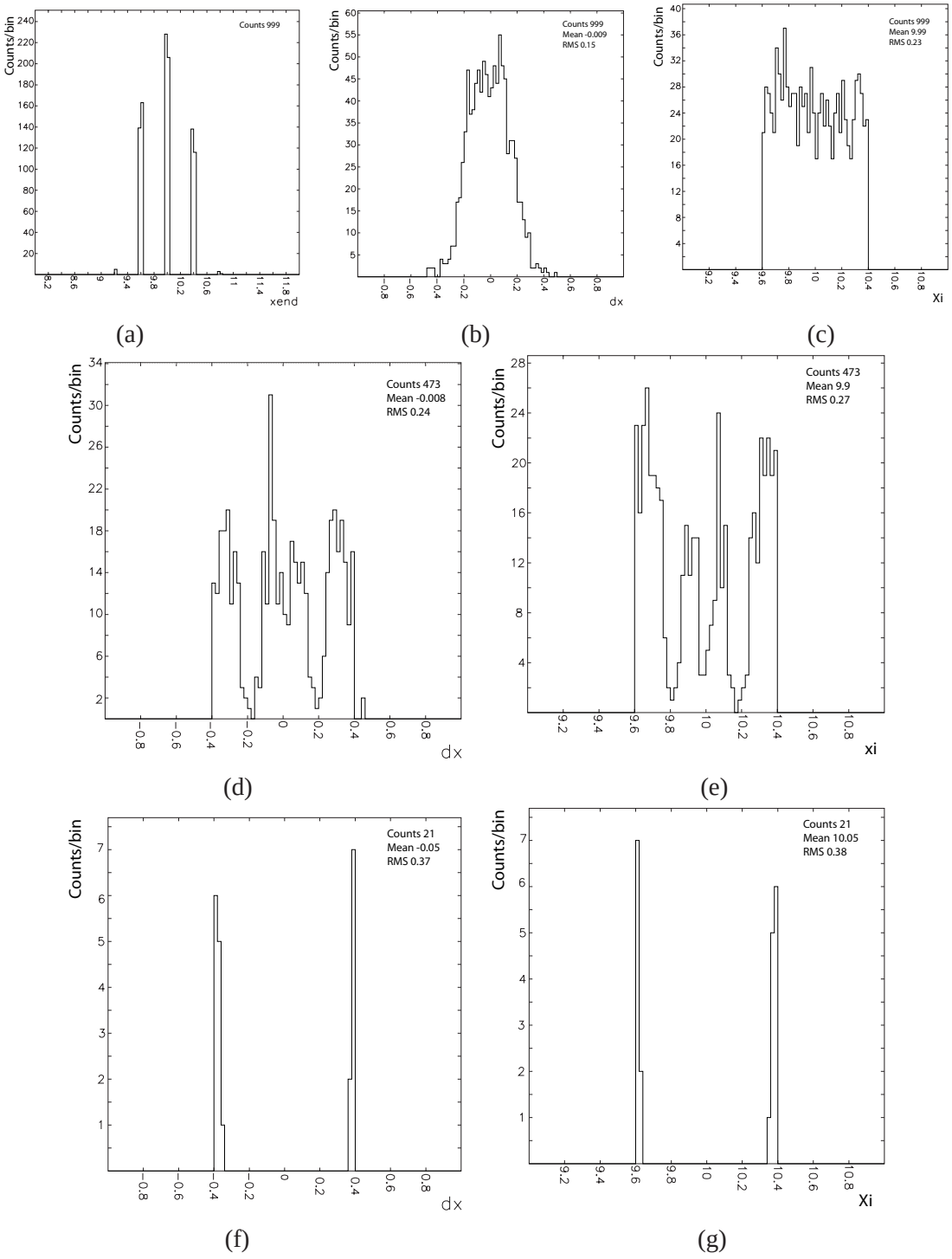

Figure 4. Histograms issued from Garfield simulations at full transparency for a, b and c, half transparency for d and e, and full opacity for f and g, with *xend* the final coordinate of the electrons, *dx* the difference between the original coordinate and the final one and *xi* the original coordinate, all distances in cm.

2012 JINST 7 P01006

Table 1. Probability of the compatibility in shape between energy histograms in the floating mask case and biased one, for the center wire and the center pad row. All the wires of the mask were biased at V_m plus the difference written in the first line. To make our results more general the corresponding relative difference is written below.

Bias difference: $V = V_m$	+10V (+0.9%)	-15V (-1.4%)	-40V (-3.8%)	-65V (-6.1%)	-90V (-8.5%)
Center wire (%)	4	7	93	22	4
Center pad row (%)	1	16	85	0	0

In all cases, MAYA was filled with 98% Helium gas and 2% CF_4 (quencher) at either 1 bar or 500 mbar.

3.2.1 Biases for transparency

The biases to be put on all the mask wires for a full transparency can be deduced from the height of the mask, assuming a homogeneous drift field: the nominal voltage V_m calculated in the previous section. For information, with our geometry, one finds -1060 V for a drift bias of -3000 V. Our first test consisted in verifying the accuracy of this estimate.

The first procedure aimed at defining the *normal* conditions and mimic the absence of mask. In both the source and the beam runs, this could be achieved by either translating the source away from the center or by turning MAYA for the beam to enter with an angle. The energy deposited and detected away from the mask is hence compared to the situation where the mask, however present, was disconnected from any bias supply and assumed floating at the potential induced by the drift electric field. By comparing the energy deposited and measured on the pads we showed that the disconnected mask, within our experimental resolution, was equivalent to removing the mask. From now on the "disconnected" mask state could be considered as a reference for transparency.

For the second part of this test the drift bias is kept constant on the cathode and the biases on all the mask wires will be changed around the transparent value V_m. The energy spectrum from both the central wire and the sum of all pads in the central row are then compared to the floating mask results. Not only the energy but also the shape similarities of the spectra are compared using a Kolmogorov-Smirnov procedure.

Results are presented in table 1. The highest similarities are found here for $V = V_m - 40$ V $\pm$ 25 V, which corresponds to a difference of -3.8% . This shift had already been observed with the simulations since the nominal value V_m had to be slightly decreased to compensate the concentric field lines close to the edge wires of the mask. Moreover, with 3000 V on the 20 cm drift gap, a misalignment of 1 mm in the height of the mask creates already a shift of 15 V in its nominal value.

3.2.2 Opacity evolution study with central mask bias

The main observable here is the number of electrons received by the amplification wires and the pads below and out of the mask. This corresponds to an experimental energy recorded by their respective electronics.

2012 JINST 7 P01006

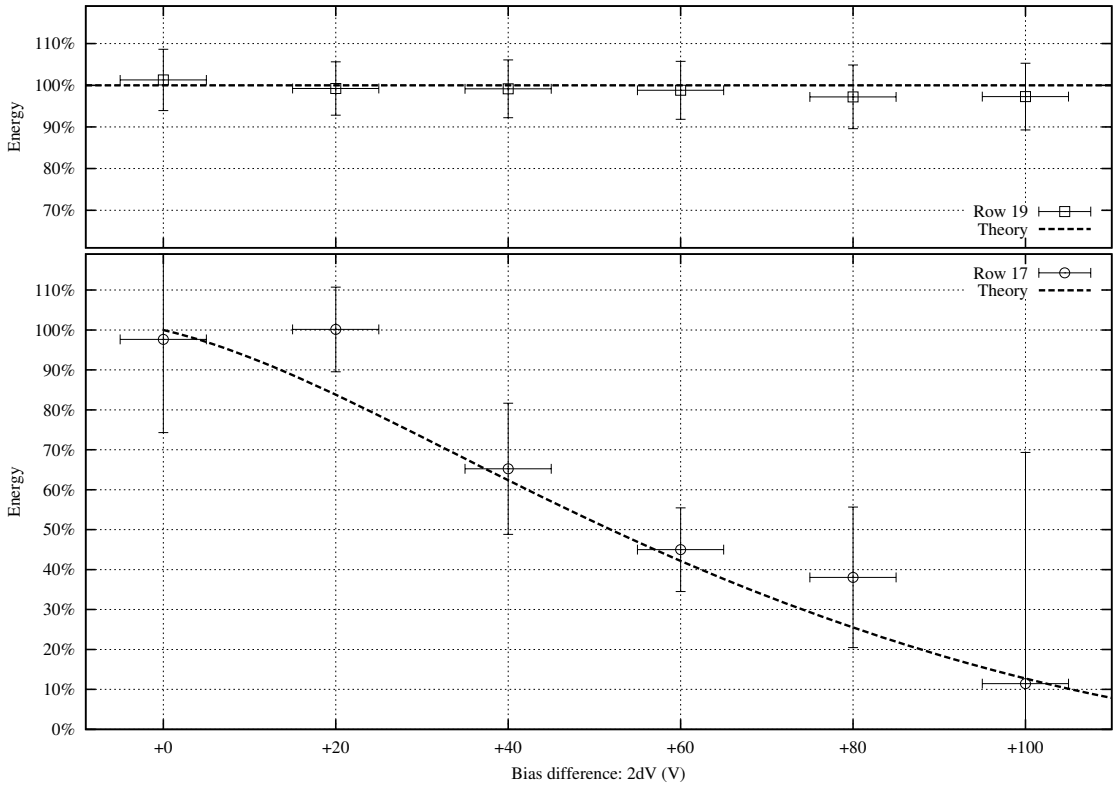

Figure 5. Energy evolution (i.e. electrons collected) measured on the central pad rows #17 (bottom view graph) and external row #19 (top) function of the bias difference $2dV$ between the center and the external wires of the mask. Simulation results are presented in dashed line.

We present in figure 5 the evolution of the energy measured on the central row of pads (#17, just below the mask) and away from it (#19) as a function of the bias difference between the inner wire of the mask and the outer ones ($2dV$). These results have been obtained with the source runs and by triggering on a silicon detector placed in front of the source at the end of the mask so as to select the most parallel tracks to the mask. The expected behavior (dashed line) is observed: applying an additional bias reduce the number of electrons reaching the pad plane by attracting them to the mask. Row #19 being away from the mask should not be affected. The number of electrons collected however slightly decreases with the mask transparency. Row #18, located closer to the mask but not exactly below, is also affected but with smaller proportion than 17 (not shown on the figure). The dashed line has been obtained by simulation. The simulation and the experimental curves are matching within the error bars. The silicon used for trigger in the source runs is bigger than the mask transversal size whereas in the simulations, the electrons were released exactly over the mask. It could explained the small differences observed between the simulation and the experimental results.

For illustration purpose, in beam results are also shown in figure 6 (right), where the measure energy distribution on the central wires is presented function of the transparency (from 100% on top to 10% at bottom). One can clearly observe the shift as well as some flattening. Note that this last effect is not of crucial importance since the beam energy in MAYA is obtained from range

2012 JINST 7 P01006

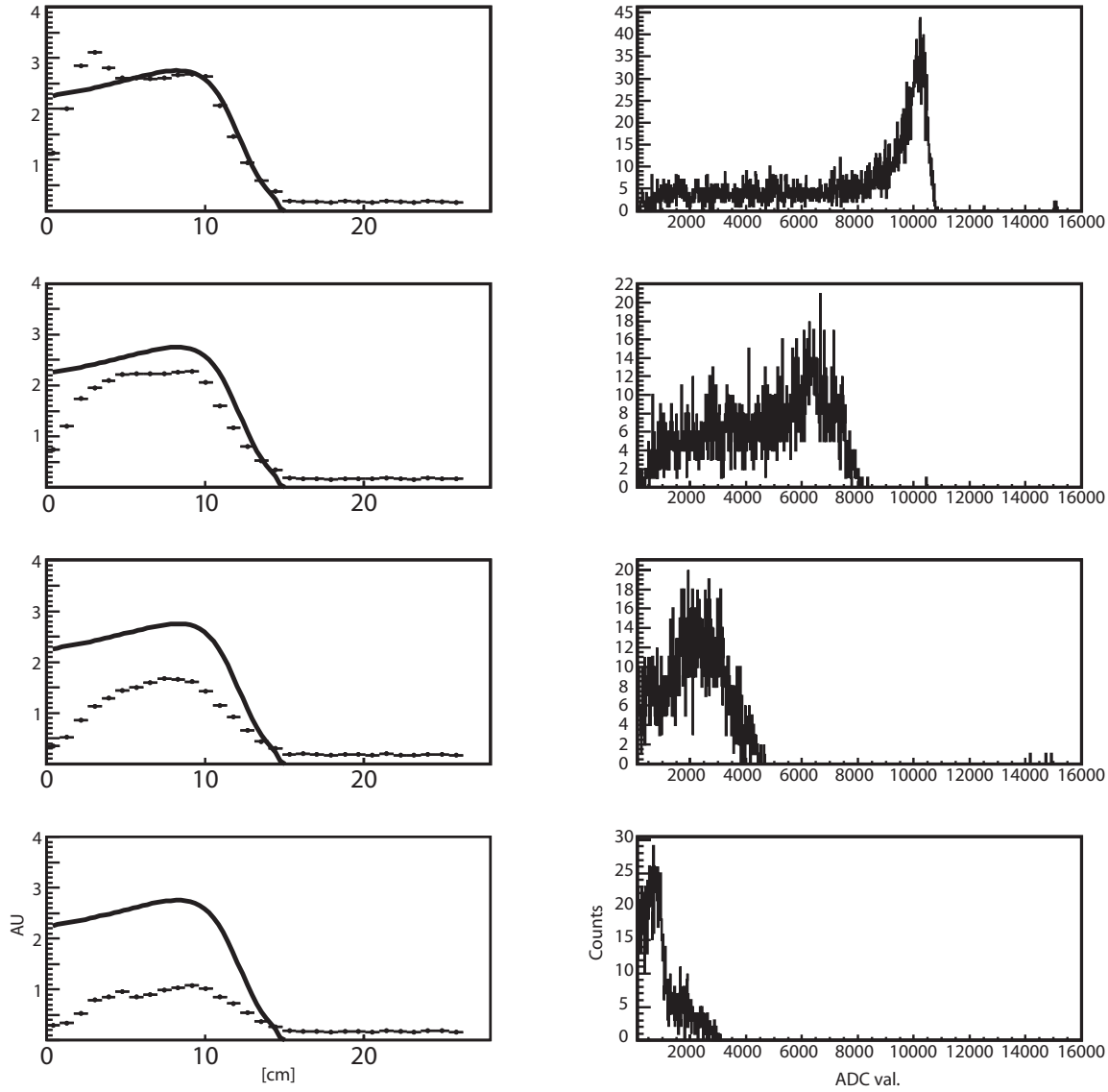

Figure 6. Experimental in-beam results using the mask and decreasing its transparency from top to bottom with: (left) beam deposited energy as a function of distance on the central pads with SRIM curve superimposed and (right) histogram of the beam deposited energy on the central wire.

measurement and not from the response amplitude of the pads or the wires.

3.2.3 Transversal dispersion, drift time and range

The use of such a device is not *a priori* without effects on the electron trajectory. In the following we investigate the various consequences on the measured energy, drift time and particle track reconstruction. The trajectory of the electrons is affected by the presence of the mask. One observable measuring its effect is the charge dispersion transversal to the trajectory. Our goal here is not to study the absolute dispersion but its relative evolution with the mask transparency. We thus build the charge distribution function of the distance to the track, event by event. The evolution

2012 JINST 7 P01006

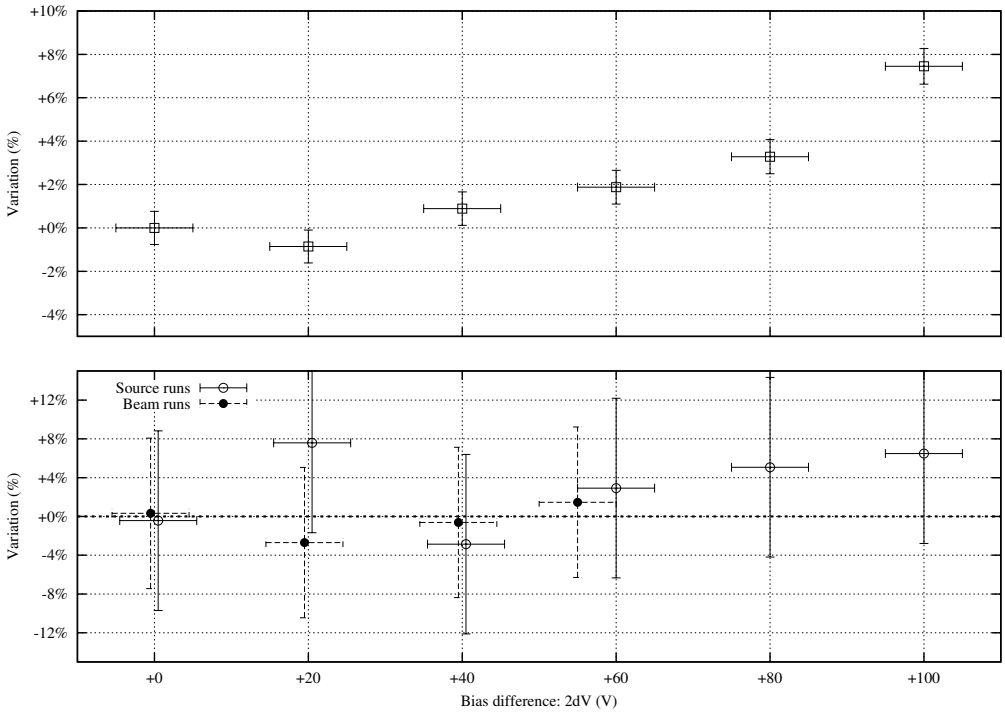

Figure 7. Transversal dispersion (bottom) and drift time (top), relative to the V_m reference case, as a function of the bias difference between the mask center wire and outer wire.

of its RMS for every bias difference is presented on figure 7 (bottom). Figure 7 (top) shows the evolution of the drift time with the bias difference. We took as reference the case where the mask was transparent.

For both curves, the mask has a weak influence. The transverse charge dispersion indicates that the field lines are not strongly deformed under and farther from the mask. Concerning the drift time, the electrons feel, once below the mask, an electric field lowered by $2 \times dV/h_m$. In He+CF_4(2%) at low electric field (100 V/cm), a variation of the electric field of 10 V/cm is equivalent to a change of 0.05 cm/μs in the drift speed which corresponds to 6% of drift velocity variation. This is the variation observed here in the drift time. The mask has an influence on the electron drift velocity and hence on the drift time, but this is without any consequence on the trajectory reconstruction.

Finally, we measured the range of beam particles as a function of the transparency, using "beam runs" data. Experimental results are illustrated in figure 6. We compare the experimental energy loss distribution as a function of the distance (left) from transparency (top) to increasing opacity (bottom), with SRIM [11] simulation (solid line). One can observe that on average the shape of the energy distribution does not change much, albeit the expected change in amplitude. Using a basic algorithm based on the half-maximum charge of the profile to calculate the stopping point of Argon beam nuclei, a more qualitative result is obtained, listed in table 2. The average distance of the stopping point is found reasonably constant independently of the opacity. Its distribution is however broadened. A better tracking algorithm adapted to the experimental situation can always be used to solve this issue [8]. However, owing to the fact that simulations show that the range measurement error is of the order of 1 mm in MAYA and that SRIM predicts longitudinal

2012 JINST 7 P01006

Table 2. Average distance from the entrance windows of the ^{36}Ar stopping point. The error is defined as the full width half maximum (FWHM) of the distribution.

Transparency	Stopping point (mm)
100%	11.1±0.7
70%	11.1±1.9
40%	11.5±2.1
10%	10.7±1.6

straggling of about 1 millimeter, we conclude that the presence of the mask does not significantly affect the measurement of the range.

4 Conclusion

A simple set-up improving the energy dynamics of active targets is presented. It uses a tunable electrostatic mask gathering partially the ionization electrons generated by the beam. Results of simulations and experimental measurements are reported and show a good agreement. This set-up has already been used successfully in nuclear physics experiments with MAYA in 2010 and 2011. A symmetrical mask gathering also the ions could be interesting in case of high energy deposits to avoid space charge effects in the drift gap.

References

[1] A. Vorobev et al., *Experimental apparatus for the study of small angle neutron-proton elastic scattering at intermediate-energies*, *Nucl. Instrum. Meth.* **A 270** (1988) 419.

[2] CH.-E. Demonchy et al., *MAYA: An active-target detector for binary reactions with exotic beams*, *Nucl. Instrum. Meth.* **A 583** (2007) 341.

[3] C. Monrozeau et al., *First Measurement of the Giant Monopole and Quadrupole Resonances in a Short-Lived Nucleus: ^{56}Ni*, *Phys. Rev. Let.* **100** (2008) 042501.

[4] B. Blank et al., *A time projection chamber for three-dimensional reconstruction of tow-proton radioactivity events*, *Nucl. Instrum. Meth.* **A 613** (2010) 65.

[5] M. Caañano et al., *Resonance state in ^{7}H*, *Phys Rev. Lett.* **99** (2007) 062502.

[6] J.C. Santiard et al., *Gasplex : a low-noise analog signal processor for readout of gaseous detectors*, CERN-ECP-94-17 (1994).

[7] H. Raether, *Electron avalanches and breakdown in gases*, Butterworth, London U.K. (1964).

[8] T. Roger et al., *Tracking algorithms for the active target MAYA*, *Nucl. Instrum. Meth.* **A 638** (2011) 134 [arXiv:1012.3560].

[9] P. Nemethy, P.J. Oddone, N. Toge and A. Ishibashi, *Gated time projection chamber*, *Nucl. Instrum. Meth.* **212** (1983) 273.

[10] R. Veenhof, http://garfield.web.cern.ch/garfield/ (1984).

[11] J. Ziegler, http://www.srim.org/ (1983).

2012 JINST 7 P01006